Kathmandu University
Journal of Science, Engineering and Technology

Aerodynamic performance analysis and evaluation of NACA 65_3-218 airfoiled aircraft at different blended winglet configurations

T. R. Pant* , S. B. Shah , and M. Kshetri

Department of Mechanical Engineering, Kathmandu University Dhulikhel, Nepal.

Abstract

The research project explores specifically airfoiled (NACA 65_3-218) wing model for its aerodynamic performance, basically, the ratio of coefficient of lift to that of drag, on adapting a non-twisted classical winglet, also known by the name of Whitcomb (blended) winglet, by configuring its geometrical parameters. After reviewing the state-of-art of this technology used in modern aircrafts both in commercial/passenger and military, the only parameter that has significant influence on the particular results we were looking for, which is the increased C_L/C_D ratio relative to clean wing, was the cant angle of the winglet. When simulated using ANSYS Fluent solver, 3D-flow at the wingtip was visualized for both winglet and without winglet cases which showed the reduced intensity of the vortex at the tip, in the former case than the latter. Gain of 8-12% was found in C_L/C_D ratio in 30° canted winglet case after solving and plotting the percentage gain in C_L/C_D ratio relative to that of clean wing without the winglet against general angle of attack, for different cases where winglet cant angle was the only variation in geometrical parameters. Validation of the results was done by performing the grid independence and the convergence tests. The results were analyzed on the basis of relation of local angle of attack along the winglet span (α_{winglet}) with the general angle of attack (α). Near vertical winglets (lower cant angle) cases were found successful in maintaining zero pressure gradient at the tip, lowering the intensity of vortex and downwash intensity but a failure in harnessing the lift force like near horizontal winglets (highly canted winglet) and vice versa.

Keywords: CFD; Winglet; Aerodynamics; Angle of attack

1. Introduction

The aircraft manufacturing industry has been evolving very generously considering the improvement in its propulsion system, service, aerodynamics, etc. in both civil and military aviation. Military and civil aircraft are different basically in their design because of their entirely different purposes. Military aircraft lack in terms of their weight carrying capacity while having a higher range factor. They are mostly designed for rescue, medical supply, firefighting, emergency issues, like purposes. Consequently, having lower takeoff speeds, lesser runway distances, quick flight time like benefits, it is much more efficient for its considered purposes. Even though they are military purpose aircraft, the thrust of achieving better fuel economy in the last two decades has influenced this arena of aviation as well. The necessity to seek higher fuel economy can be expected by the fact that the graph of fuel price is continuously going up as shown by Fig. 1. Applications for winglets have spread far beyond commercial and military aviation and well into the personal aircraft market [1].

In comparison with other types of transportation fuel, jet fuel takes up a major portion of the total fuel consumption and is expected to grow by 64 % from 2017 to 2050 according to the last annual energy outlook report [2]. As per the BTS, U.S. passenger airlines' collective net profit increased by 18.1 billion dollars in 2015 [3] mostly due to lower kerosene-based aviation fuel expenses in 2015 as compared to 2014.

It has been noted that transportation is fundamentally 0% efficient as it involves moving mass from rest at one point to rest at another point so that the energy of the system is unchanged. That it does take energy to accomplish this objective is due to the presence of drag, and the reduction of drag has been a primary focus of aircraft design over the last century. At present, airlines pay hundreds of millions of dollars in fuel costs annually, and the environmental impact of aircraft is closely tied to the amount of fuel required, so the accurate estimation and reduction of this drag are of great interest.

Winglets allow for drastic improvements in aircraft fuel efficiency, range, stability, and even control and handling. They are traditionally considered to be near-vertical, winglike surfaces that can extend both above and below the wingtip where they are placed. However, one may see them today as also being associated with any wingtip device intended to enhance wingtip performance.

Blended winglets are merely designed to appear as naturally coming out of wingtips to reduce the interference drag at the wing-winglet junction. They are estimated to cost around $600,000 for an 8-foot set and are mostly used to save fuel rather than fly faster [5]. A 1-percent fuel saving at cruise conditions can save up to 12 gallons of fuel saved per hour. This represents tens of thousands of gallons of saved fuel and hundreds of thousands of dollars saved in a single year.

How good can the performance enhancement be? Well, some designs have seen astounding improvements, like 7-percent gains in the lift-to-drag ratio and a 20-percent reduction in drag due to lift at cruise conditions. Wingtip technologies still hold great promise for aeronautics today and well into the future, with the potential to save hundreds of thousands of dollars in fuel costs per aircraft

*Corresponding author. Email: panttilakraj@gmail.com

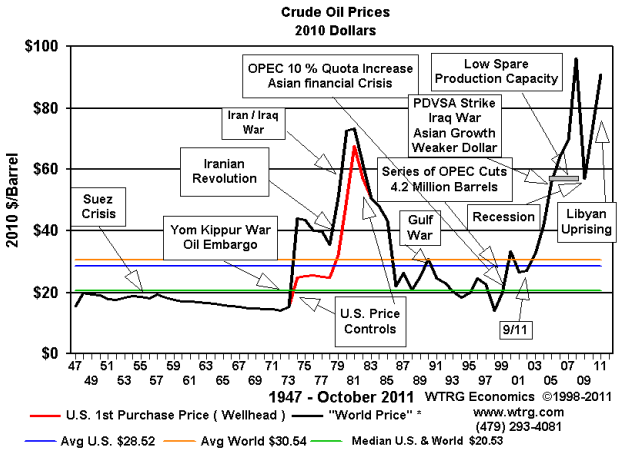

Figure 1: Fuel prices evolution [4].

each year [6].

There are two fundamental ways to deal with the design and analysis of engineering systems involving fluid flow; experimentation and calculation. The former typically involves building models and testing in wind tunnels or other available facilities, physically in a lab and the latter involves solving differential equations either analytically or computationally. Both the methods are used to complement each other, where experimentation is used to obtain global properties like lift, drag, pressure drop, power while CFD to obtain the details about the flow field, such as shear stresses, velocity, and pressure profiles, and flow streamlines. Besides, experimental data are often used to validate CFD solutions by matching the computationally and experimentally determined global quantities.

In this work, the computational domain for a specifically airfoiled aircraft wing has been modeled using the student version of ANSYS FLUENT. The geometrical dimensions of the modeled domain have been verified by the fact that there are no drastic velocity/pressure gradients at the outermost region of the domain. The conditions (Mach number) applied for the simulation purpose are based on the information available regarding the specific military aircraft we have considered. However minor details like considering the properties changes of air in the particular cruise conditions have been neglected. Four different wingtip conditions (clean wingtip extension, winglet added wingtips at 20°, 30°, 45° cant angles) have been simulated for the study.

1.1. Science of wingtips

Before we can understand how winglets work, we must first understand the problem they are intended to solve. Extremely hazardous and detrimental effects can be created at the tip of every wing. The severity depends on many factors, such as how much lift is being produced and how fast the wing is passing through the air. These effects usually take the form of a vortex trailing the tip of the wing.

A vortex is the rotational motion of a fluid medium, in this case air, generated as the high-pressure air from the bottom of the wing flows around the tip-side edge to the lower pressure region on top. While vortices known as bound vortices are created along the entire length of the wingspan, it is the trailing vortices behind the wingtips that are much stronger due to the three-dimensional effect of a finite wingspan. Such a phenomenon can create significant stability and efficiency issues for the entire aircraft. For high-lift, low-speed conditions as seen on runways, or for high subsonic cruising speeds, the drag induced from these vortices can account for up to half of all drag [6].

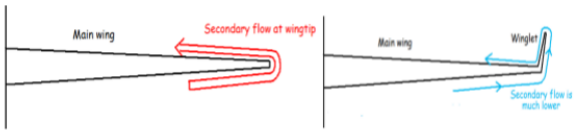

Figure 2: Influence of winglets to the secondary flow at the wingtip.

Equation of the total drag of a wing is a sum of the parasite drag and the induced drag. In terms of non-dimensional coefficient of drag it is

$$C_D = C_{D0} + C_{\mathrm{Di}}$$

Here C_{D0} is the drag coefficient at zero lift which is independent of lift, known as parasite drag coefficient. The second term is called the lift-induced drag coefficient, C_{Di}, defined as:

$$C_{\mathrm{Di}} = \frac{C_L^2}{\pi\, AR\, e}$$

$$\mathrm{AR} = \frac{s^2}{S_{\mathrm{ref}}}$$

Increasing the aspect ratio of the wing is one well known technique applied to reduce these vortices. Theoretically infinite wings do not produce these types of vortices. As an aircraft cannot have infinite wing the only way to prevent this wingtip vortices are to create an obstacle which will prevent the secondary flow in the wingtip. This obstacle to the high-pressure air to produce any type of secondary flow is winglet. Providing a winglet to a wing the wingtip vortices is shifted from wing to winglet and such vortices has lesser intensity and thus reduces the induced drag which helps to increase the overall lift to drag ratio of an aircraft. The influence of winglets on the secondary flow of a wing is illustrated by Fig. 2.

Manufacturers have developed different methods to counteract this action. Winglets can be added to the tip of an aerodynamic profile to reduce this flow. These fins act by preventing the formation of the vortex. The winglets can be at the top or bottom of the profile. Another method to counteract the flow is to fine tune the tip of the profile, reducing the pressure difference and softening the air flow around the tip.

From an engineering point of view - and ultimately that of mission capability and operating economics – the main purpose and direct benefit of winglets is reduced airplane drag.

2. Materials and method

2.1. Winglet design space

A classical Whitcomb winglet, which we are considering for our purpose of the study has at least six geometrical parameters: sweep λ, cant ψ and twist ξ angles, the height h, fillet radius R, and the taper ratio B = b/b_0 (Fig. 3). In the coordinate system z-axis denotes the wing span direction perpendicular to the aircraft (XY) symmetry plane, x-axis: the direction of flight, and y-axis normal to XZ plane: the normal force direction.

It is not viable to explore by varying every geometrical parameter manually and compiling results for each dimensional combinations to see the benefits on the overall C_L/C_D. According to the optimization techniques used in [7], for airfoiled winglets, C_L/C_D is mostly sensitive to cant angle ψ, where a high fidelity cant angle ψ CFD and mathematical optimization was prioritized over other geometrical parameters to get a cost-effective, 'multi-fidelity' approach. Thus, the aerodynamic performance of the wing was analyzed based on the cant angle alone.

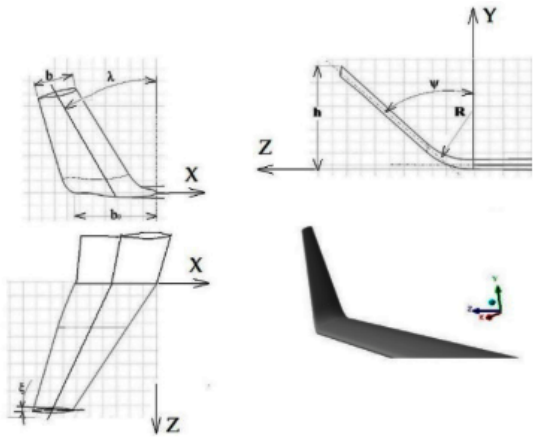

Figure 3: Geometrical parameters of a typical Whitcomb winglet [7].

Table 1: Geometrical dimensions of the wing.

Planform area	0.35 m^2
Tip chord (Ct)	0.2 m
Root chord (Cr)	0.5 m
Mean Aerodynamic Chord (MAC)	0.35 m
Aspect ratio (AR)	2.86
Taper ratio	0.4
Cross-section (or airfoil)	NACA 65(3)-218
Span (b)	1 m
Leading-edge sweep angle	16.69°

2.2. Modeled Geometry, Computational Domain

All the geometrical dimensions chosen for modeling the wing and the winglet as tabulated in Table 1 and Table 2 are taken after scaling the actual wing dimensions. For instance the actual wingspan of a typical military aircraft is 25 m but, according to Table 1, dimension of span (b) is taken as 1 m, scaling down the actual model by a factor of 25. However, ratios like taper ratio , AR are considered as original aircraft since those parameters must not be scaled preserving the actual model of the aircraft. Similarly, dimensions of a typical Whicomb's winglet has been scaled according to the scale factor applied in the wing. Table 3 has the wetted area of the different cases that has been compared. A slight difference in the area at different winglet cant angle can be observed in the table, since the change in the cant angle requires a slight change at the transition from wingtip to the winglet-tip. In Fig. 4, top view of winglet transition from wingtip developed in the design modeler can bee seen.

To model the variable cant angle winglet, an extension to the baseline wing was added. Then, the cant angle is modeled by adding a curvature radius at the wingtip join with the winglet, in such a way as to guarantee a smooth transition between the wing and the winglet. The winglet span used in this study corresponds to 20% of the wingspan of the baseline wing. This value was chosen based on previous studies conducted by different authors [8–10] where they suggest the use of winglet's span values between 10% and 20% of the wingspan.

A sketch of the computational domain and the boundary conditions layout is shown in Fig. 5. The far-field boundary in this figure corresponds to a Dirichlet type boundary condition and the outflow to a Neumann type boundary condition. The boundaries were placed far enough (body of influence shown in Fig. 6) from the wing surface so there are no significant gradients normal to the surface boundaries. The wing was modeled as a no-slip wall,

Table 2: Geometrical dimensions of the winglet.

Planform area	0.0225m^2
Winglet span	Blended arc length (0.08 m) + trailing straight edge (0.1 m) = 0.2 m
Tip chord	0.1 m
Root chord	0.2 m
Taper ratio	0.5
Radius of curvature of blended area	0.1 m

Table 3: Wetted area of wing modeled in design modeler.

Wing type	Wetted area
Clean wing	0.72338 m^2
Cant angle 45°	0.788352 m^2
Cant angle 30°	0.791264 m^2
Cant angle 20°	0.793988 m^2

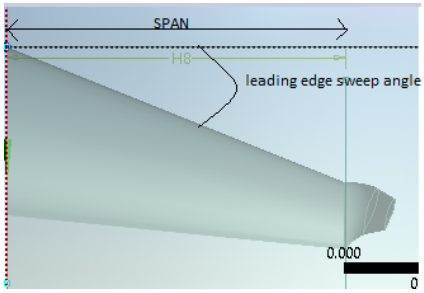

Figure 4: Wingspan, leading-edge sweep angle, and planform area.

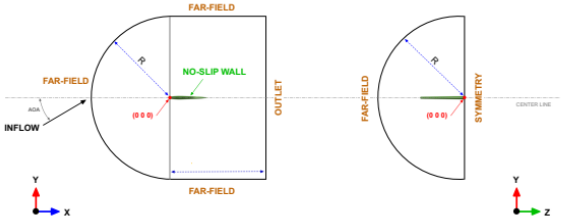

Figure 5: Computational domain and boundary conditions.

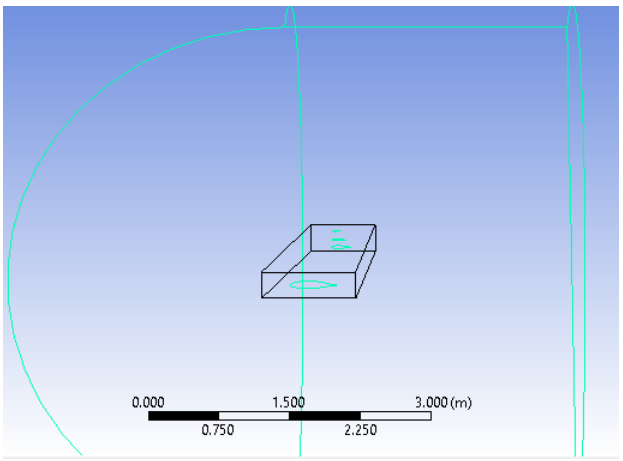

Figure 6: Body of influence enclosing wing geometry.

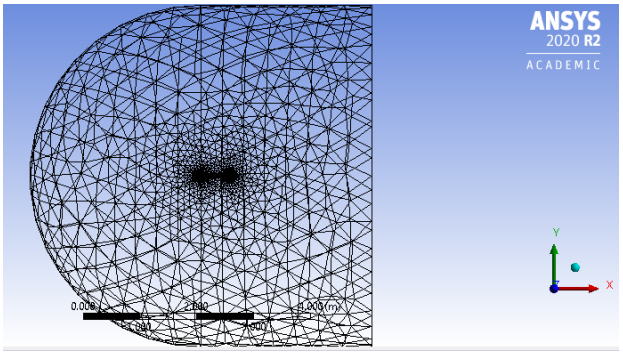

Figure 7: Generated mesh and view of the bullet-shaped domain.

where we used continuous wall function boundary conditions for the turbulence variables. In all cases, the average distance from the wing surface to the first cell center of the surface is approximately four viscous wall units ($y+ \approx 4$). A hybrid mesh was used for all the simulations, with prismatic cells close to the wing surface and tetrahedral cells for the rest of the domain. A typical mesh is made up of approximately 512000 cells (also the limit of student version fluent solver), depending on the winglet's cant and sweep angle.

2.3. Mesh

Since the number of elements that can be solved in the student version of Ansys Fluent is up to 512,000, the total number of elements in mesh was limited to this number. The software automatically generated tetrahedral, pyramid, and wedge structured mesh. However proper refinement and the desired mesh was obtained by the use of the following controls.

By using explicit sizing controls, the resolution of the geometry can be accurately captured and we can ensure that we accurately resolve any high gradient areas in the flow, such as wake or separation/recirculation zones. Fig. 7 shows the entire domain and the mesh after refinement while Fig. 8 shows the mesh in the surface of the wing (close up view).

The Body Sizing control also can use geometric bodies themselves to control the mesh refinement. A body of influence can be of any arbitrary shape/size and intersects the main fluid domain that we are trying to mesh. The fluid domain involved this control with the body of influence as the enclosure for the wing-body. In the intersection region, the ANSYS Mesher uses this body of influence to create the right amount of local mesh refinement. This smart feature also removes the need to decompose the main body into complicated sub-regions. Mesh size = 0.5m, growth rate 20%

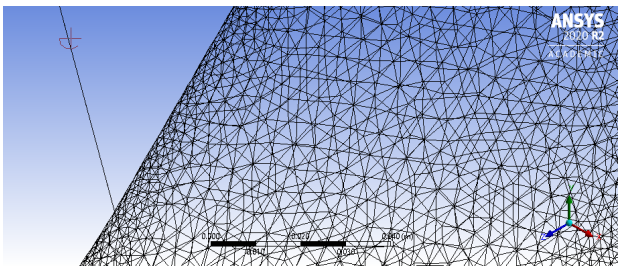

Figure 8: Wing surface mesh.

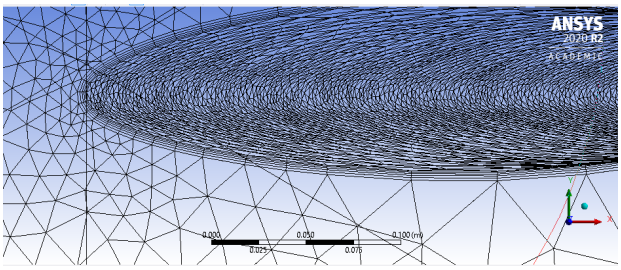

Figure 9: Inflation: boundary layer.

Face Sizing in ANSYS Meshing has also been used to apply a face sizing to the wing surface to control the mesh size on those particular faces to make them more refined and capture the curvature features of the wing surface. This is one of the more common ways to control the mesh and ensure that a consistent, high-quality mesh is being created at the wing surface.

Mesh size = 0.05m growth rate 20%

Curvature capture local minimum size = 0.002m

The inflation attribute of mesh sizing was used on the fluid-wing surface interface to capture the no-slip boundary phenomenon properly. This control creates finer inflation layer mesh on the selected boundary faces so that the influence of boundary layer can be captured (Fig. 9), thus making the first cell center within $30 \leq y+ \leq 300$ wall units in all cases for the use of non-equilibrium wall function. A pre-inflation algorithm was applied to generate the mesh in which the surface mesh will be inflated first, and then the rest of the volume mesh will be generated.

Maximum thickness = 0.005m, 5 layers.

Mesh quality was determined as the average and minimum value for orthogonal quality was no less than 0.73639 and 0.0403. The maximum number of elements with a low value of aspect ratio was a reference for a properly generated mesh. In all cases, the maximum value for aspect ratio was27.08 with an average value of 3.86. A bar graph showing the number of cells corresponding to different aspect ratio can be seen in Fig. 10.

2.4. Turbulence Modelling

The k-epsilon (k-ϵ) model for turbulence has been set up in our solver which is the most common to simulate the mean flow characteristics for turbulent flow conditions. It belongs to the Reynolds-averaged Navier Stokes (RANS) family of turbulence models where all the effects of turbulence are modeled.

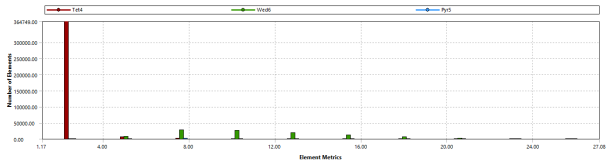

Figure 10: Aspect ratio: elements in the clean wing case.

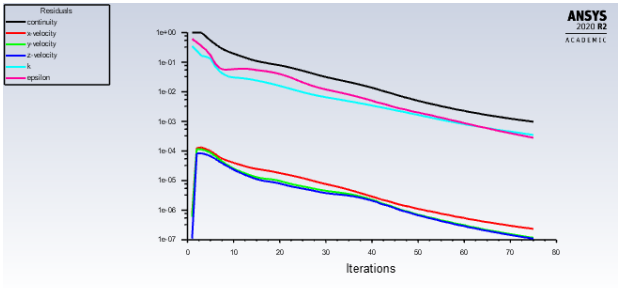

Figure 11: Residuals converging to tolerable limits with iterations at 1% turbulence.

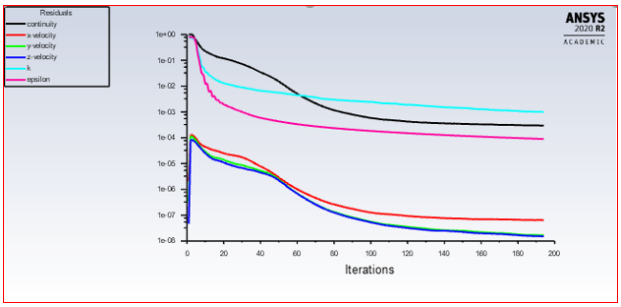

Figure 12: Residuals converging to tolerable limits with iterations at 5% turbulence.

It is a two-equation model. That means that in addition to the conservation equations, it solves two transport equations (PDEs), which account for the effects like convection and diffusion of turbulent energy. The two transported variables are turbulent kinetic energy (k), which determines the energy in turbulence, and turbulent dissipation rate (ϵ), which determines the rate of dissipation of turbulent kinetic energy. To solve the additional two equations, it takes turbulent intensity (I) that outputs k, turbulence model constant C_μ which usually takes the value of 0.09 and turbulent length scale l to output ϵ.

The k-ϵ model is shown to be reliable for free-shear flows, such as the ones with relatively small pressure gradients, but might not be the best model for problems involving adverse pressure gradients, large separations, and complex flows with strong curvatures.

During the parametric study, the angle of attack (α) was changed by adjusting the incidence angle value of the inlet velocity and all forces were computed in the reference system aligned with the inlet velocity. The free stream velocity was taken to be 110 m/s in accordance with the average cruising speed of a turboprop military aircraft. All the computations were initialized using free-stream values and the incoming flow is characterized by a turbulence intensity value equal to 1.0%. All the turbulence variables were initialized following the guidelines given in references [11,12].

Fig. 11 and Fig. 12 compare the rate with which the residuals go down to the set limit depending upon the turbulence intensity we initialize in the inlet and outlet boundary. In our case, when the turbulence was set to 1%, the solution was more stable than when we set it to be 5%. It took, residuals, nearly 200 iterations to fall within the tolerable set limit which was in the order of 10^{-3} while the same tolerance limit was achieved in about 70 iterations when it was initialized with 1% turbulence.

2.5. Mathematical model of the Winglet local flow field

Given that the winglet is an airfoiled finite-span lifting surface, finite wing theory can be applied to describe the three-dimensional flow field in its vicinity. For analysis of the results and explanation for the obtained values, winglet surface local flow field has been quantitatively analyzed through the term local angle of attack (α_{winglet}) which is different in different general angle of attack for wing (α) than the wing, which is related by

$$\alpha_{\text{winglet}} = K_\varphi * \alpha$$

considering non-twisted winglet and withdrawing the α_{flow_field} term from the actual local angle of attack expression. K_φ is a cant coefficient accounting for the local winglet angle of attack (α_{winglet}) for a different general angle of attack (α) which is linked to the ψ as follows, increasing α for a vertical winglet (ψ = 0) does not have any effect on α_{winglet}, while the change in the general angle of attack is equal to the local winglet angle of attack for a horizontal winglet ($\psi = \frac{\pi}{2}$), $\Delta\alpha_{\text{winglet}}^{\text{horizontal}} \approx \Delta\alpha$. Mathematically, for $K_{\varphi=0} = 0$, while for a horizontal winglet $\psi = \frac{\pi}{2}$, $K_\varphi = 1$. Solving the system of equations,

$$K_\varphi = \frac{\psi}{\frac{\pi}{2}}$$

Only positively canted winglets were considered in this paper, where ψ is ranged from $0 \le \psi \le \frac{\pi}{2}$, which implies: $0 \le K_\varphi \le 1$. It can be verified for a half-canted winglet ($\psi = \frac{\pi}{4}$): $K_{\varphi=\frac{\pi}{4}} = \frac{\frac{\pi}{4}}{\frac{\pi}{2}} = 0.5$. This means that for any increase of the general angle of attack, half of that increase will contribute to geometrically increasing the winglet angle of attack: $\Delta\alpha_{\text{winglet}} = 0.5\Delta\alpha$.

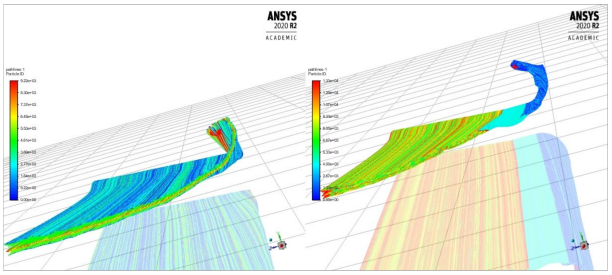

Figure 13: 3D flow at wingtip of a clean wing (left) and a winglet added wing (right).

3. Results and discussion

3.1. Particle pathlines comparison

To visualize the 3D flow at the wingtip, particle pathlines were generated as shown in the figure below.

In two different cases, clean wingtip and winglet tip, the vortex at the latter case can be observed to be diminished than the former. We can see a vortex of higher strength in the left part of the image at the tip where there is no winglet, than in the image at the right side where the vortex is more concentrated/shifted higher.

Moreover, the effect of 3D flow can be seen in the base section of the two differently configured wings in the images. The upper side of the wing without a winglet is throughout affected by the 3D flow causing a loss in pressure gradient (ultimately lift coefficient) while the energy is recovered by shifting and limiting the vortex to tip by adding a winglet as seen in the right image of Fig. 13. The flow that causes loss or induces a drag component of force is less effective in winglet added cases as shown by the images.

3.2. Impact of winglet cant angle on C_L/C_D ratio

After the geometries and meshes for each case were generated and refined accordingly, every case was solved in the academic version of Ansys Fluent solver at different angles of attack. C_L/C_D ratio calculated was plotted against angle attack and compared in a single graph.

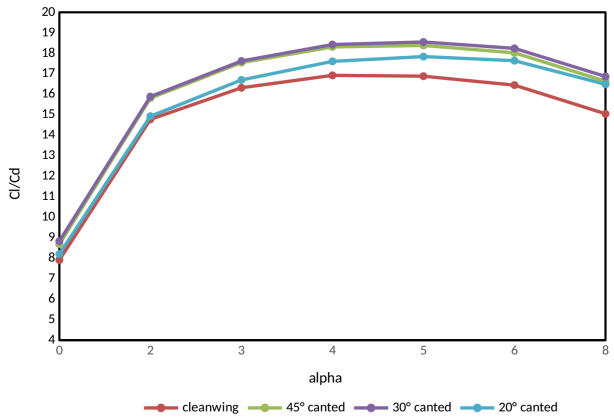

Figure 14: C_L/C_D ratio compared at different angles of attack for different wing configurations.

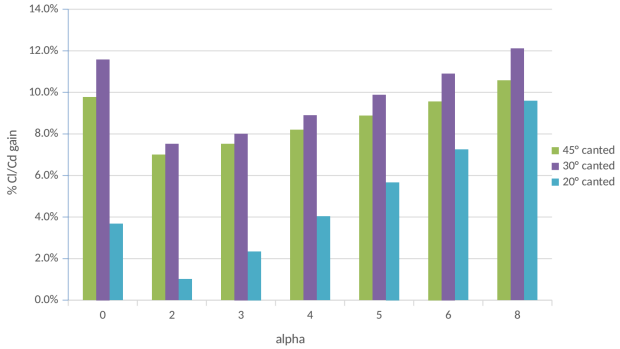

Figure 15: Percentage gain in $\mathbf{C_L/C_D}$ ratio after adapting differently canted winglet at clean-wingtip at different angles of attack.

From Fig. 14 we can say the ratio is significantly lower (below 16) and sensitive to lower angles of attack, 0-3 degrees, while it has increased and flattened within 16-18 is less sensitive to the angle of attack for 3-6 degrees. It can also be inferred from the graph below that there is no significant benefit achieved in winglet added cases compared to that of clean wingtip case, the graph looks nearly overlapped for every case in 0-3 degrees angle of attack.

Although, the highest C_L/C_D value, which is about 18.5, is achieved in the case of 30° canted winglet case at 5° angle of attack, it is not the exact case where the percentage gain in C_L/C_D ratio (Fig. 15) is highest relative to the clean wing as we can see the curve for clean wing drops much significantly as the angle of attack increases beyond 5°. This drop in the ratio is only observed in the clean wing case, while the curve is still flat in winglet added cases. At a higher angle of attack 5-6° for the clean wing, the increased lift coefficient results in higher lift dependent drag (induced drag), which caused significant loss in C_L/C_D ratio. But for a similar case in winglet added cases, we have seen no drop in the ratio, no matter how much the lift coefficient has increased and resulted in the induced drag. This is why the percentage gain in the ratio relative to the clean wing is higher at an 8° angle of attack.

At a lower angle of attack, the graph for 20° canted winglet and the clean wing suggests that there are no benefits realized when adding near-vertical winglets (20° canted) at a lower angle of attack (0-3°), but as we increase α further, we can see significant gain improvement in the ratio by adapting even the near-vertical winglet. At lower cant angles, the local angle of attack for such winglets is very insignificant at a very small general angle of attack and does not contribute to the lift coefficient as discussed in the mathematical model of the winglet local flow field (materials and methods).

Comparing the percentage gain in the ratio for different winglet

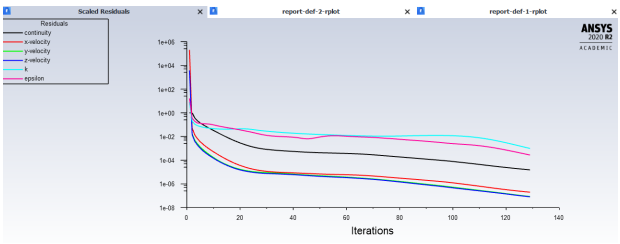

Figure 16: Residual graph for clean wing.

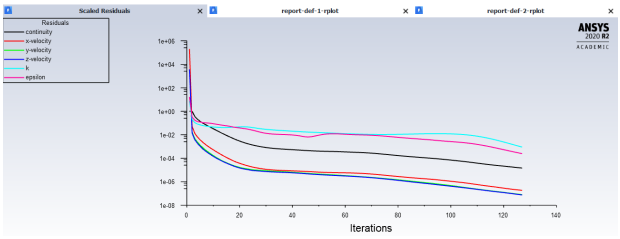

Figure 17: Residual graph for clean wing with 5% refined mesh size.

cases, we see that, winglets near-vertical cases are very sensitive to change in cant angle. The gain is maximum for 30° canted winglet case in every angle of attack case we have. In 20° canted winglet case, which is nearly vertical compared to other cases, can better handle the induced drag component, however, as the local angle of attack is very low, we lose our lift component which results in a penalty in the ratio and consequently the gain relative to the clean wing. A higher cant angle would lose its capability to restore the lost energy by vortex generation even though the local angle of attack is high enough to generate a higher lift coefficient. As we have seen in the case of 45°, increasing the cant angle, more like a horizontal winglet than 30°, would result in induced drag, and ultimately would penalize $\mathbf{C_L/C_D}$ ratio.

3.3. Validation

Grid independence test was performed on the clean wing geometry at 0° angle of attack to determine that the further refinement of the mesh is unnecessary for comparison of the different winglet added wings as the solution has no significant change in value after further refinement of the mesh by 5% of the initial mesh size under the same convergence criteria. In compliance with the independence test, Fig. 16 and Fig. 17 show that there is no difference in the residual graphs for the two cases.

The first case with 471315 number of elements in the mesh: the result of the simulation in this case as the lift to drag ratio is 7.9.

Second case: Clean wing simulation with 5% refinement in mesh size(501425elements): the result of the simulation as the lift to drag ratio in this case is 7.9.

This shows the independence of the CFD result concerning the grid size for up to the first decimal place of the lift to drag ratio, which is acceptable for our purpose of lift to drag ratio comparison of different winglet added wings. The residual graph in both cases shows the solution converges after no more than 130 iterations under an absolute convergence limit of 0.001for the values of continuity, k, epsilon and, x, y, and z velocity components. Same convergence criteria with a similar-sized grid were used for all the other cases.

Test for convergence of the solution is another technique to verify the CFD results. For example, a report graph has been inserted below in Fig. 18 to show the positively tested convergence test in a 30° canted winglet at a 2° angle of attack case. This is how every solution has been verified in the solver for all the cases.

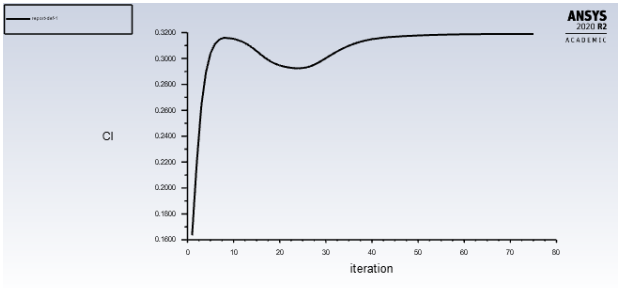

Figure 18: An illustration of a converged solution.

4. Conclusion

The following conclusion is made from the strength of this research work

- Adapting a classical Whitcomb's winglet to a clean wing tip enhances the lift to drag ratio as compared to the clean wing tip extension.
- Neither near vertical or horizontal winglets are absolutely efficient, instead a definite winglet cant angle can result optimum lift to drag ratio.
- 30° canted winglet was found most successful while compared to other winglet cant angles presuming the trend of the other near vertical or horizontal winglet adaptation by analyzing few cant angle cases.
- Variable local angle of attack along the winglet span could be more efficient design than a simple winglet considered in the research.

References

[1] Bargsten, C, *Winglets: Striving for Wingtip Efficiency*, In B. Clayton, & M. Gibson, NASA Innovation in Aeronautics: Select Technologies That Have Shaped Modern Aviation (pp. 11-12). Washington, DC: NASA (2011).

[2] US EIA, *Annual Energy Outlook 2018 with Projections to 2050*, U.S. Energy Information Administration, Washington, DC (2018).

[3] Bureau of Transportation Statistics, *Airline Fuel Cost and Consumption* (U.S. Carriers - Scheduled), U.S. Department of Transportation, Washington, DC (online).

[4] Williams J L, Fuel Prices Evolution, WTRG Economics, London, Arkansas `http://www.wtrg.com/oil_graphs/oilprice1947.gif`.

[5] Allward M, Wingtip Technology, *J. Motum, Putnam Aeronaut. Rev.*, 1 (1989) 41.

[6] Chambers J R, Concept to Reality: Contributions of the NASA Langley Research Center to U.S. Civil Aircraft of the 1990s, *NASA SP-2003-4529*, (2003).

[7] Gueraiche D & Popov S, Winglet Geometry Impact on DLR-F4 Aerodynamics and an Analysis of a Hyperbolic Winglet Concept, *Aerospace*, 4 (2017) 23.

[8] Whitcomb R T, *A design approach and selected wind tunnel results at high subsonic speeds for wing-tip mounted winglets*, NASA Technical Note (TN), Washington, DC. (1976) NASA TN D-8260.

[9] Shollenberger C A, *Application of an Optimized Winglet Configuration to an Advanced Commercial Transport*, NASA, Hampton, Virginia. (1979) NASA Contractor Report 159156.

[10] Smith L A & Campbell R L, *Effects of Winglets on the Drag of a Low-Aspect-Ratio Configuration*, NASA, Hampton, Virginia. (1996) NASA Technical Paper 3563.

[11] Wilcox D C, Turbulence Modeling for CFD, La Cañada Flintridge, CA (2010).

[12] Menter F R, Two-equation eddy-viscosity turbulence models for engineering applications., *AIAA J.*, (1994).